THE ROLE OF COAL ASH IN THE CORROSION PERFORMANCE OF STRUCTURAL ALLOYS IN SIMULATED OXY-FUEL ENVIRONMENTS

K. Natesan and Z. Zeng
Argonne National Laboratory, 9700 South Cass Avenue, Argonne, IL 60439
E-mail: natesan@anl.gov; Telephone: (630) 252-5103; Fax: (630) 252-8681

June 2012

Paper presented at the 26th Annual Conference on Fossil Energy Materials, Pittsburgh, PA, April 17-19, 2012 and to be published in the conference proceedings.

*Work supported by the U.S. Department of Energy, Office of Fossil Energy, Advanced Research Materials Program, Work Breakdown Structure Element ANL-4, under Contract DE-AC02-06CH11357.

THE ROLE OF COAL ASH IN THE CORROSION PERFORMANCE OF STRUCTURAL ALLOYS IN SIMULATED OXY-FUEL ENVIRONMENTS

K. Natesan and Z. Zeng
Argonne National Laboratory, 9700 South Cass Avenue, Argonne, IL 60439
E-mail: natesan@anl.gov; Telephone: (630) 252-5103; Fax: (630) 252-8681

Abstract

The U.S. Department of Energy (DOE) Office of Fossil Energy is intensely promoting research and development of oxy-fuel combustion systems that employ oxygen, instead of air, for burning the fuel. The resulting flue gas primarily consists of H_2O and CO_2 that facilitates sequestration of CO_2 or use it in a turbine to generate electricity, thereby leading to reduction in CO_2 emissions. Also, as the oxidant is bereft of N_2, NO_x emissions are minimized to a great extent from the exhaust gas. Studies at NETL have indicated that oxy-fuel combustion can increase efficiency in the power plants from the current 30-35% to 50-60%. However, the presence of H_2O/CO_2 and trace constituents like sulfur and chlorine in the gas environment and coal ash deposits including alkalis at the operating temperatures and pressures can have adverse effects on the corrosion and mechanical properties of structural alloys. Thus, there is a critical need to evaluate the response of structural and turbine materials in simulated H_2O/CO_2 environments in an effort to select materials that have adequate high temperature mechanical properties and long-term environmental performance.

During the past few years, we have conducted corrosion tests on a variety of candidate alloys in CO_2 and steam containing environments in the presence of SO_2, typical of oxy-fuel combustion systems. Materials selected for the study include intermediate-chromium ferritic steels, Fe-Cr-Ni heat-resistant alloys, and nickel-based superalloys. We presented detailed results on the corrosion performance of various alloys after exposure at 750°C. During the current year, we continued testing of alloys to evaluate their performance in a simulated oxy-fuel environment with low pO_2 and the presence of simulated coal ash consisting of alumina, silica, and iron oxide along with sodium and potassium sulfates. In addition, we have examined the role of CaO in the ash (typical of US Western coal ash) in laboratory exposure environments. Detailed results are presented on weight change, scale thickness, internal penetration, microstructural characteristics of corrosion products, and cracking of scales for the alloys after exposure at 750°C. To establish the role of steam in the exposure environment, tests were also conducted in environments with and without steam in the oxy-fuel gas atmospheres. Results from these tests are used to address the role of steam in the long-term corrosion performance of alloys.

1. Background

An increase in carbon dioxide gas in the atmosphere is identified as one of the major causes for the global climate change and one of the sources of carbon dioxide is the exhaust from fossil fuel fired combustion power plants. The energy production, in particular electricity generation, is expected to increase globally due to population increase and per capita increase in energy consumption. To meet the energy needs, fossil fuels (coal, oil, and gas) will play a major part in production even

with a projected increase in alternate renewable sources. However, to minimize the carbon dioxide emission, the current systems emphasize its capture from power plants and subsequent sequestration. The oxy-fuel combustion systems (without the diluent nitrogen gas) can enable recycling of the carbon dioxide to the compressor, use of novel gas turbines, and advance reuse. The U.S. department of Energy/Office of Fossil Energy is supporting the development of combustion systems replacing air with nearly pure oxygen with a goal to achieving a near zero-emission coal-based power system. For this purpose turbines and combustor technologies that use pure oxygen in fuel combustion are being developed. The major advantage of combustion under pure oxygen is the potential for separation and capture of CO_2 and for achieving power system efficiencies in the range of 50 to 60%.

In previous years, we evaluated the corrosion performance of candidate materials in CO_2, steam, steam-CO_2 mixtures, and air [1-4]. Materials selected for the study include intermediate-chromium ferritic steels, Fe-Cr-Ni heat-resistant alloys, and nickel-based superalloys. Coupon specimens of several of the alloys were exposed to pure CO_2 and to CO_2 plus steam environments at temperatures between 650 and 950°C for times up to 10,000 h. We presented detailed results on the corrosion performance of various alloys after exposure at 750°C. The data showed that the weight change for all the alloys was small when tested in all four environments. Among the alloys, Alloy 800 exhibited the most weight gain in all four environments. In general, high nickel and Ni-base alloys exhibited less oxidation than the Fe-base alloys in all exposure environments. The high silicon alloys such as Alloys 330 and 333 showed superior corrosion resistance in pure CO_2 environment when compared their performance in CO_2-steam or pure steam environments. The volatilization of silicon oxides in steam-containing environments may be the cause for this increased corrosion. We also addressed the mechanism for the oxidation of various alloys in these environments and also evaluated the long-term performance of the alloys from the standpoint of scaling and internal penetration. The oxidation test results showed that the total corrosion (scaling plus internal penetration) rates are <0.05 mm/y at 750°C, in the absence of ash or sulfur.

In the past year, we performed corrosion tests to evaluate the corrosion performance of the structural alloys in the presence of simulated coal ash consisting of alumina, silica, and iron oxide along with sodium and potassium sulfates. Detailed results were presented on weight change, scale thickness, internal penetration, microstructural characteristics of corrosion products, and cracking of scales for the alloys after exposure at 750°C [5]. To establish the role of steam in the exposure environment, tests were also conducted in environments with and without steam in the oxy-fuel gas atmospheres. Results from these tests were used to address the role of steam in the long-term corrosion performance of alloys. During the current year, we continued the corrosion experiments in the presence of ash (rich in iron oxide) that simulates U.S. Eastern coal and also initiated tests in environment to simulate the ash (rich in calcium oxide) that would be derived from US Western coal. The former is rich in iron oxide while the latter is rich in calcium oxide.

2. Experimental Procedure

Materials

The compositions of the alloys selected for the study are listed in Table 1. Several alloys, both ASME coded and uncoded, were selected for corrosion evaluation. The alloys included

advanced ferritic steel modified 9Cr-1Mo and austenitic Fe-base alloys Types 304 and 330 stainless steel and Alloy 800H. In addition, several high-Ni alloys (333, 617, 625, 602CA, 230, 693, 740, and 718) were included in the study, especially for application at temperatures above 700°C. MA956 is a Fe-Cr alloy produced via mechanical alloying and subsequent extrusion. Apart from fireside and steam side corrosion resistance, the alloy selected for application in steam superheaters and reheaters should possess adequate strength at elevated temperatures for the duration of service.

Table 1. Nominal composition (in wt.%) of alloys selected for corrosion study

Material	C	Cr	Ni	Mn	Si	Mo	Fe	Other
253MA	0.09	20.9	10.9	0.6	1.6	0.3	Bal	N 0.19, Ce 0.04
800H	0.08	20.1	31.7	1.0	0.2	0.3	Bal	Al 0.4, Ti 0.3
333	0.05	25.0	45.0	-	1.0	3.0	18.0	Co 3.0, W 3.0
617	0.08	21.6	53.6	0.1	0.1	9.5	0.9	Co 12.5, Al 1.2, Ti 0.3
625	0.05	21.5	Bal	0.3	0.3	9.0	2.5	Nb 3.7, Al 0.2, Ti 0.2
602CA	0.19	25.1	62.6	0.1	0.1	-	9.3	Al 2.3, Ti 0.13, Zr 0.19, Y 0.09
230	0.11	21.7	60.4	0.5	0.4	1.4	1.2	W 14, Al 0.3, La 0.015
693	0.02	28.8	Bal	0.2	0.04	0.13	5.8	Al 3.3, Nb 0.67, Ti 0.4, Zr 0.03
740	0.07	25.0	Bal	0.3	0.5	0.5	1.0	Co 20.0, Ti 2.0, Al 0.8, Nb+Ta 2.0
718	-	19.0	52.0	-	-	3.0	19.0	Nb 5.0, Al 0.5, Ti 0.9, B 0.002
MA956	-	20.0	-	-	-	-	Bal	Al 4.5, Ti 0.5, Y_2O_3 0.6
WASP	0.02	20	Bal	0.5	0.75	4.3	2.0	Co 12-15, Ti 2.6-3.25, Al 1.0-1.5, Zr 0.1
ANL Alloy 1	0.2	25	71.4	-	-	-	0.7	Al 2.3, Ti 0.3, Zr 0.2, Y 0.1
ANL Alloy 2	0.2	25	71.1	-	-	-	-	Al 3.3, Ti 0.3, Zr 0.2, Y 0.1

Gas composition

To understand the effect of gas composition on alloy corrosion, in the past alloys were exposed to six different gas mixtures in the corrosion tests. Results from these exposures were reported in earlier conference [4]. During the current year, we have used two gas mixtures A and B whose compositions are listed in Table 2. These gas mixtures contain the same concentrations of O_2 and SO_2, but Gas A contained steam and Gas B had no steam. The effect of steam on the corrosion of alloys is studied by comparing the performances of alloys in the gas environments with and without steam.

Table 2. Gas composition for experiments

Gas #	CO_2 (%)	H_2O (%)	O_2 (%)	SO_2 (%)
A	68.14	26.9	3.97	0.99
B	95.04	0	3.97	0.99

Synthetic Ash Experiments

The synthetic coal-ash deposit, that simulates ash from U.S. Eastern coal, consisted of a mixture of reagent-grade SiO_2, Al_2O_3, and Fe_2O_3 in the ratio of 1:1:1 by weight. The alkali sulfate mixture consisted of Na_2SO_4 and K_2SO_4 in the ratio of 1:1 by weight. The synthetic coal-ash

deposit, that simulates ash from U.S. Western coal, consisted of a mixture of reagent-grade 36%SiO_2-16%Al_2O_3, 9%Fe_2O_3, and 29%CaO. The alkali sulfate mixture consisted of Na_2SO_4 and K_2SO_4 in the ratio of 1:1 by weight in the ratio of 1:1:1 by weight.

The specimens were buried in the ash that was contained in an alumina boat. The experiments were generally stopped after approximately every 300 h, the specimens were cooled to room temperature, cleaned of the ash by brushing, and weighed. Specimen exposures were continued with a fresh supply of ash mixture. The specimen temperature was controlled to within ≈3°C.

Upon completion of the corrosion kinetics experiments, the specimens were examined by optical metallography and by a scanning electron microscope (SEM) equipped with energy-dispersive X-ray analyzer. In some cases, the deposit materials and the scales (developed on alloy specimens) were analyzed by X-ray diffraction. Optical examination of cross sections of exposed specimens and analyses with the SEM were used to identify the morphological features of corrosion-product phases in the scale layers and to establish the thickness of scales and depth of intergranular penetration, if any, in the alloys.

3. Results and Discussion

Results on the corrosion performance of structural alloys after exposure to simulated oxy-fuel gas environments with and without steam (in the absence of ash) was reported in the last conference [5].

Figure 1 shows a plot of the relative stability of various oxide and spinel phases as a function of temperature. Also shown in the figure are the oxygen partial pressures established by the CO_2 and steam environments. It is evident that all the relevant (to alloy protection) oxide and spinel phases will be thermodynamically stable in both exposure environments. Therefore, the phases that form in the thermally grown scale will be influenced predominantly by the alloying elements present in the alloy rather than by the oxygen partial pressure in the exposure environment.

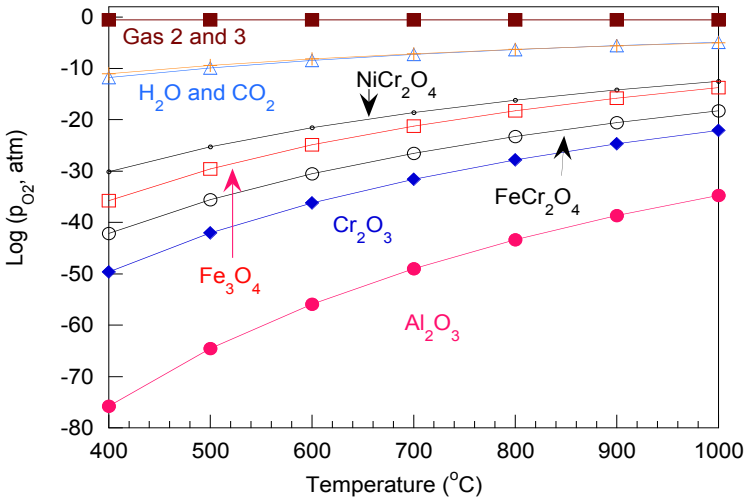

Figure 1. Thermodynamic stability of various oxide and spinel phases. Also shown are the pO_2 curves for pure CO_2 and pure steam.

In general, high nickel alloys exhibited less oxidation than the Fe-base alloys in the same exposure environments; also, alloys containing high chromium and high aluminum also exhibited superior corrosion performance. Alloys 617, 625, 230 and 718 lost weight after exposure to the gas with steam, but none of them lost weight after exposure to the gas without steam. The results indicate that steam exacerbates the spallation of oxide scales on these alloys and leads to continued oxidation.

The exposed specimens were also analyzed to evaluate the total corrosion (scale thickness and penetration) for all the alloys after exposure at 750°C in 96.03% CO_2-3.97% O_2 and 68.63% CO_2-27.4% H_2O-3.97% O_2. Figure 2 shows the penetration rates for several alloys tested at 750°C in 96.03% CO_2-3.97% O_2 and 68.63% CO_2-27.4% H_2O-3.97% O_2, assuming a parabolic kinetics. Results showed that all of the alloys exhibit total corrosion rate of <0.05 mm/y at 750°C. In general, the alloy penetration rates after exposure to the gas with steam are faster than that after exposure to the gas without steam. However, if the alloys contain niobium, the trend is reversed.

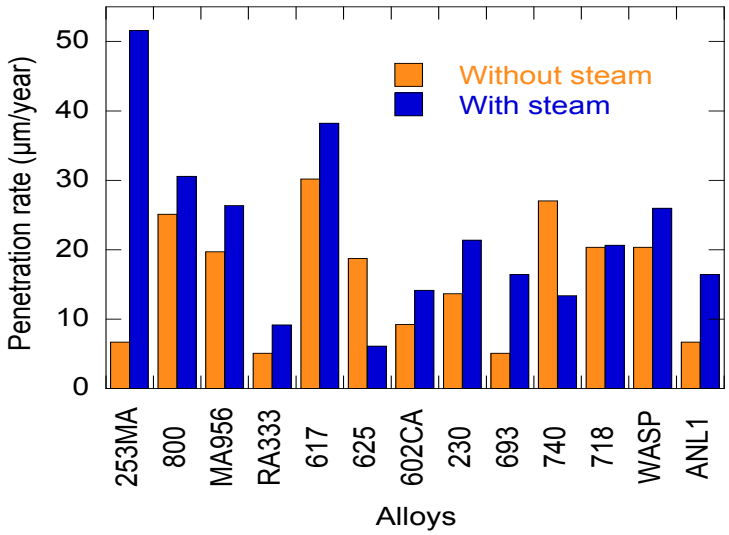

Figure 2. Penetration rates for alloys tested in 96.03% CO_2-3.97% O_2 and 68.63% CO_2-27.4% H_2O-3.97% O_2 at 750°C.

Performance in the presence of ash constituents simulating US eastern coals

Corrosion experiments in the presence of simulated coal ash and alkali sulfates were conducted at 750°C in Gas A for a total exposure time of >6000 h. Specimens were retrieved and weighed periodically and the ash was replenished every 300 h of exposure. Alloys 153MA, 253A, and 617 showed uniform attacks, after exposure in the experiment with steam. However, most alloys (Alloy 800H, MA956, RA333, 625, 602CA, 230, 718, WASP, and Alloy1) were locally attacked. Alloy 693, 740, and Alloy 2 were not attacked.

Figure 3 shows the weight loss data for several alloys tested in the presence of ash simulating US Eastern coal and Gas A at 750°C. Many of the alloys exhibit an incubation period, during which the corrosion rate is low. Upon exceeding the incubation period, the corrosion accelerated and the process followed a linear kinetics. Metallic networks were also observed in the corroded region.

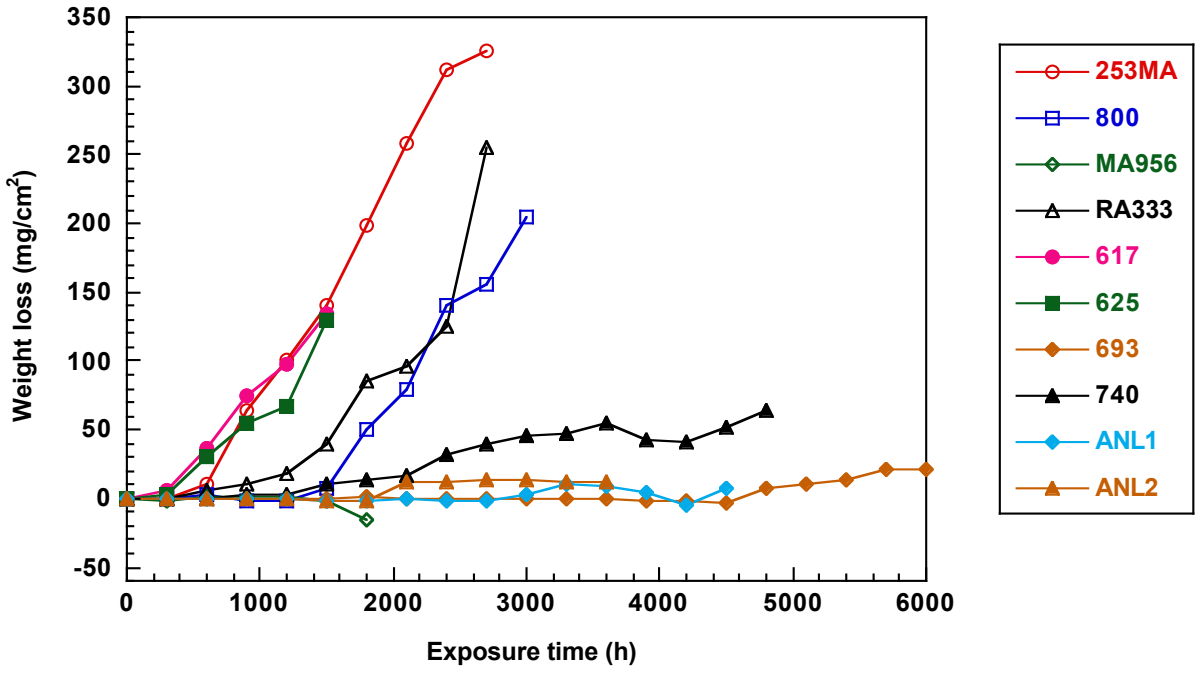

Figure 3. Weight loss for alloys, after exposure to synthetic ash (simulating US Eastern coal) and Gas A at 750°C.

The effect of steam on the incubation time depends on alloy composition and can range widely based on the test conducted in the environments with and without steam (Fig. 3). In general, the incubation times of high Cr and Ni alloys such as 693, 740, Alloy1, and Alloy2 are long. The incubation times of alloys with Nb, W and Mo are short. Aluminum addition does not benefit in ash corrosion. High aluminum alloys such as MA956, 617, 625, 602CA, 230, exhibited a shorter incubation time.

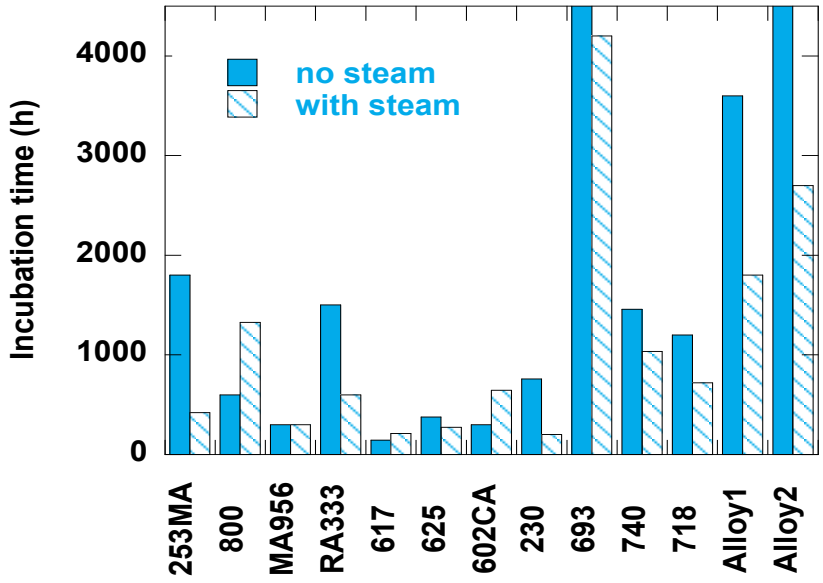

Figure 3. Incubation times for several alloys after exposure to ash (simulating US Eastern coal) plus alkali sulfates in Gas A at 750°C.

Figure 4 shows the rate of corrosion penetration for alloys in the presence of ash simulating US Eastern coal and Gas A and B at 750°C. The penetration rates of alloys after exposure to ash are much higher than that after exposure to the gas environment without ash [5]. In general, the linear penetration rates for the alloys range between 1.2-11.2 mm/y, the least being for Alloy 740 and the highest for Alloy 602CA. Alloy 446 was exposed only for short period and the penetration rate may be an underestimate. Figure 5 shows a comparison of penetration rates for Alloy 740 obtained in the current study with those reported by Baker and Smith [6] The ANL data were obtained at 750°C whereas the data of Baker and Smith were obtained at 569 and 627°C, with relatively shorter exposure times.

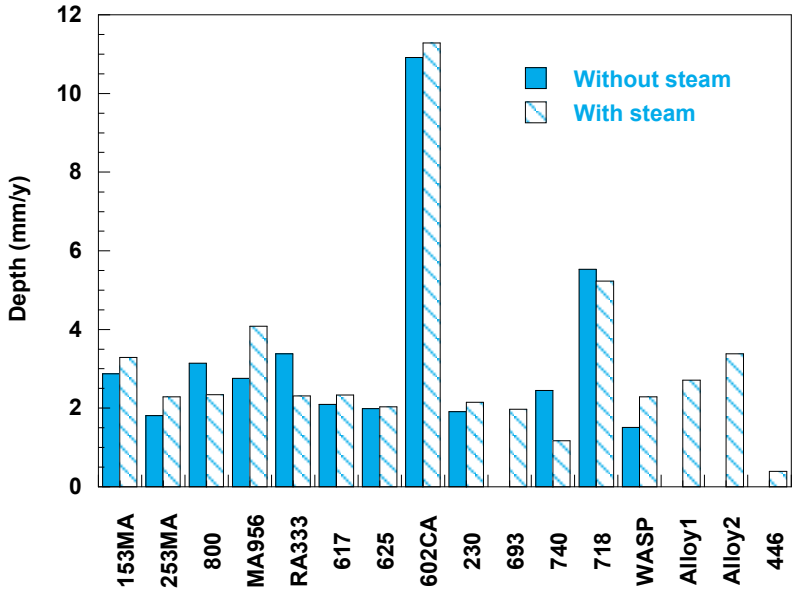

Figure 4. Corrosion depth rate data (after subtracting incubation time) for alloys after exposure to ash (simulating US Eastern coal) plus alkali sulfates in Gas A at 750°C.

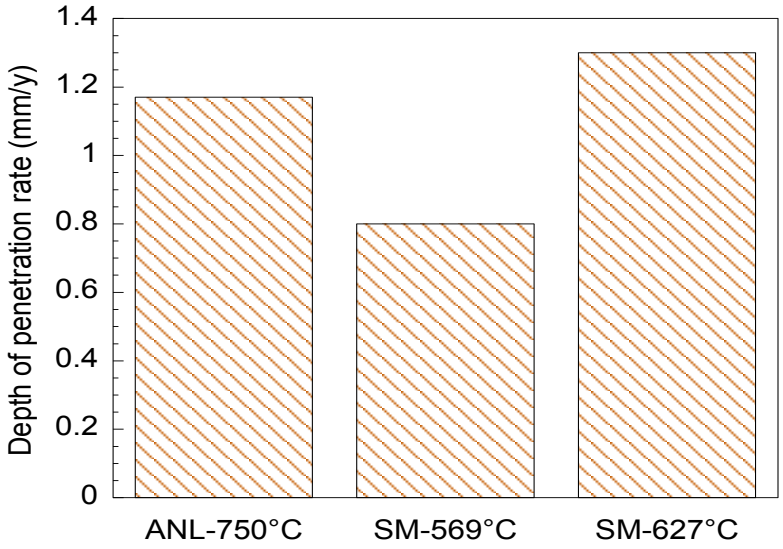

Figure 5. Comparison of corrosion depth rate data for Alloy 740 tested at ANL and at Special Metals [6].

Microstructural Observations

The surfaces and cross sections of many of the corrosion-tested specimens have been examined in detail using scanning electron microscopy and energy dispersive X-ray analysis. In some cases, the scales and ash have been analyzed using X-ray diffraction. In this paper, microstructural data are presented only for limited alloys such as Alloy 740 and Alloy 693. In the earlier paper [5], microstructural data were presented for the alloy after 600-h exposure at 750°C and concluded that the alloy performs well in oxy-fuel and ash environment. Further, its performance in the gas environment without steam was judged better than that in the gas containing steam. Localized attack was also reported on alloy 740 after exposure at 750°C. Accumulation of niobium and sulfur at the local attacked region seemed to retard the formation of a dense chromium oxide scale.

During the past year, the microstructures of specimens of Alloy 740 (after 4800-h exposure) and Alloy 693 (after 6300-h exposure) were examined using SEM and EDX. Figure 6 shows microphotographs of Alloy 740 surface and cross section. Figure 7 shows the SEM image and EDX mapping for Al, Cr, Nb, O, Co, Ni, S, and C in the corroded scale region. It is evident that substantial amount of sulfur is segregated at the interior of the scale, indicating the Cr-rich oxide scale is not protective enough to minimize corrosion in the presence of ash and SO_2. Figure 8 shows the EDX mapping in the scale/interface region, clearly indicating stringers of sulfides embedded within the scale. As the Cr-rich sulfides form, the nickel is rejected which forms a network within the scale that can enable faster transport of potential corrosion-accelerating agents.

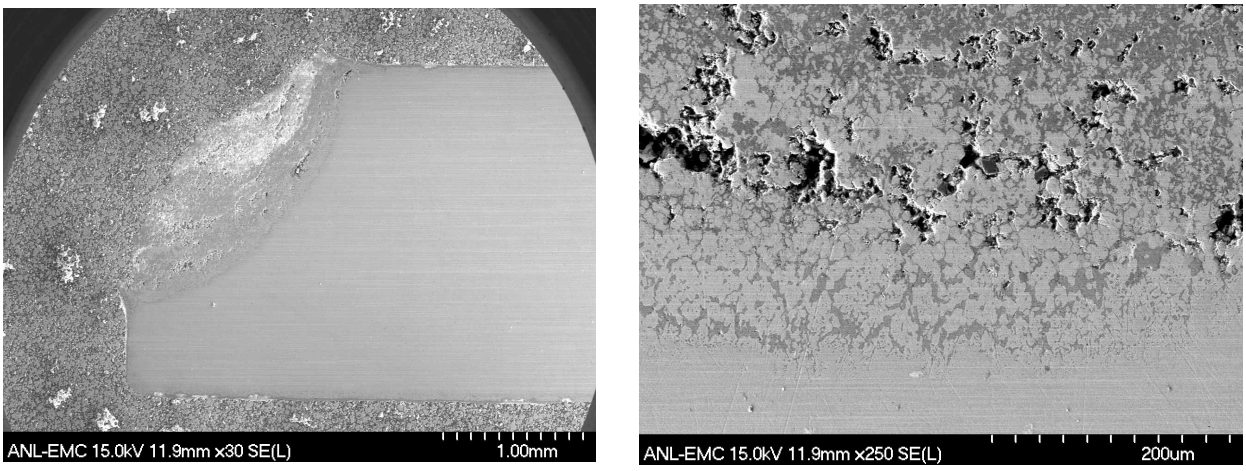

Figure 6. SEM photomicrographs of surface and cross section of Alloy 740 after 4800-h exposure to ash (simulating US Eastern coal) and SO_2 (Gas A) environment at 750°C.

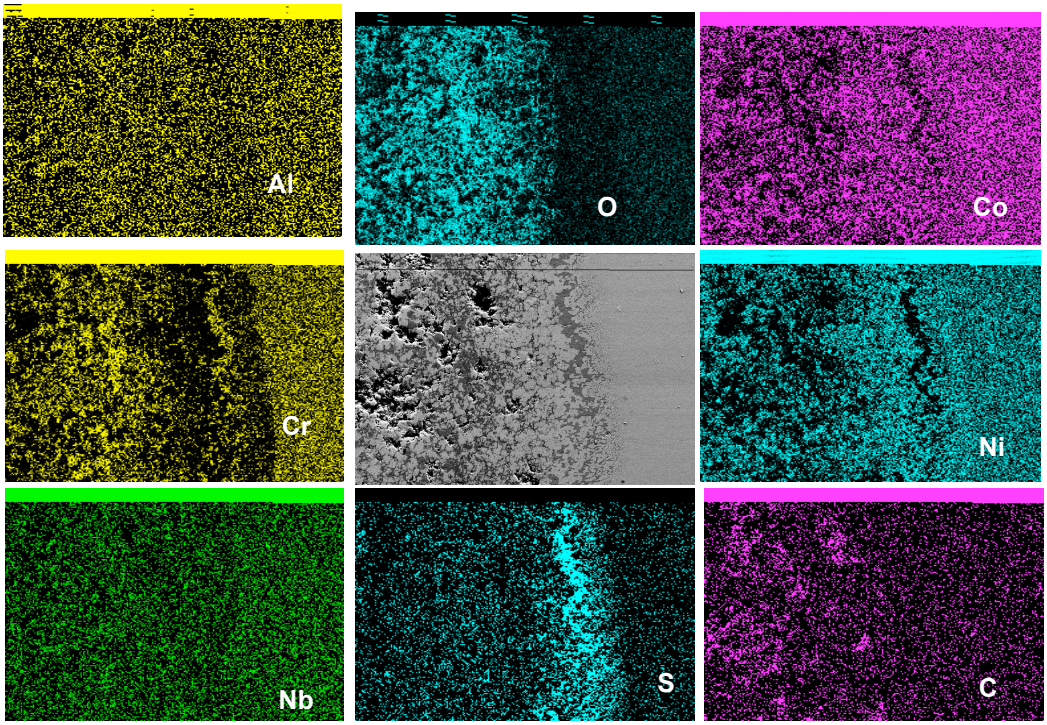

Figure 7. EDX mapping of the cross section of Alloy 740 after 4800-h exposure to Gas A and ash at 750°C.

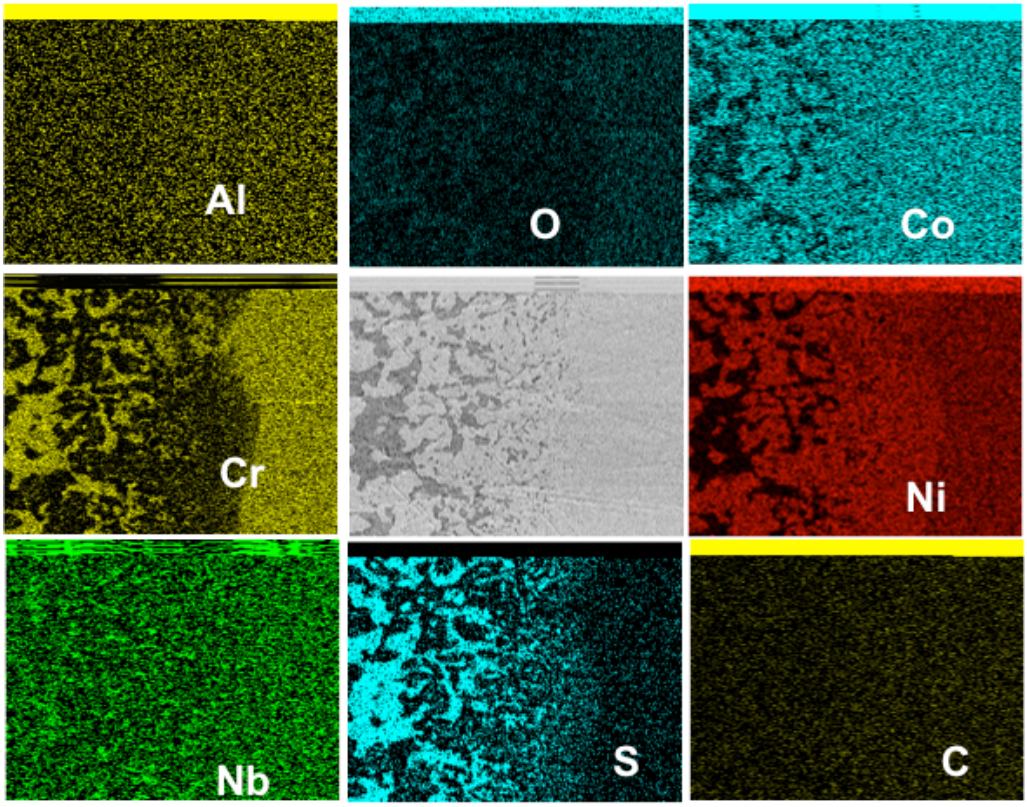

Figure 8. EDX mapping of scale/alloy interface region of Alloy 740, after 4800-h exposure to Gas A and ash at 750°C.

Figure 9 shows the SEM photomicrographs of cross sections of corroded and non-corroded regions of Alloy 693 after 6300-h exposure at 750°C. Figures 10 and 11 show the SEM images and EDX mapping for Ni, Cr, Na, O, S, Fe, and Al in the corroded and non-corroded scale regions of Alloy 693, respectively. In the corroded region (see Fig. 10), the EDX analysis shows a non-protective Cr oxide and regions of Fe and Ni rich metallic phases. The sulfur from the ash and mixture and from the gas environment seems to react with Cr to form Cr sulfides or Cr-rich oxy-sulfides in the scale leading to accelerated attack of the alloy. Internal oxidation of Al to Al oxide can be seen which has little effect on minimizing sulfidizing corrosion.

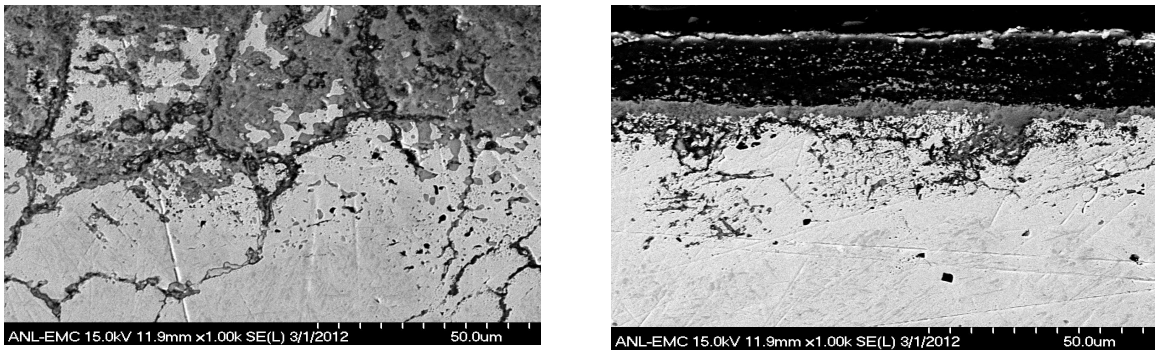

Figure 9. SEM photomicrographs of cross sections of (left) corroded and (right) non-corroded regions of Alloy 693 after 6300-h exposure to ash (simulating US Eastern coal) and SO_2 (Gas A) environment at 750°C.

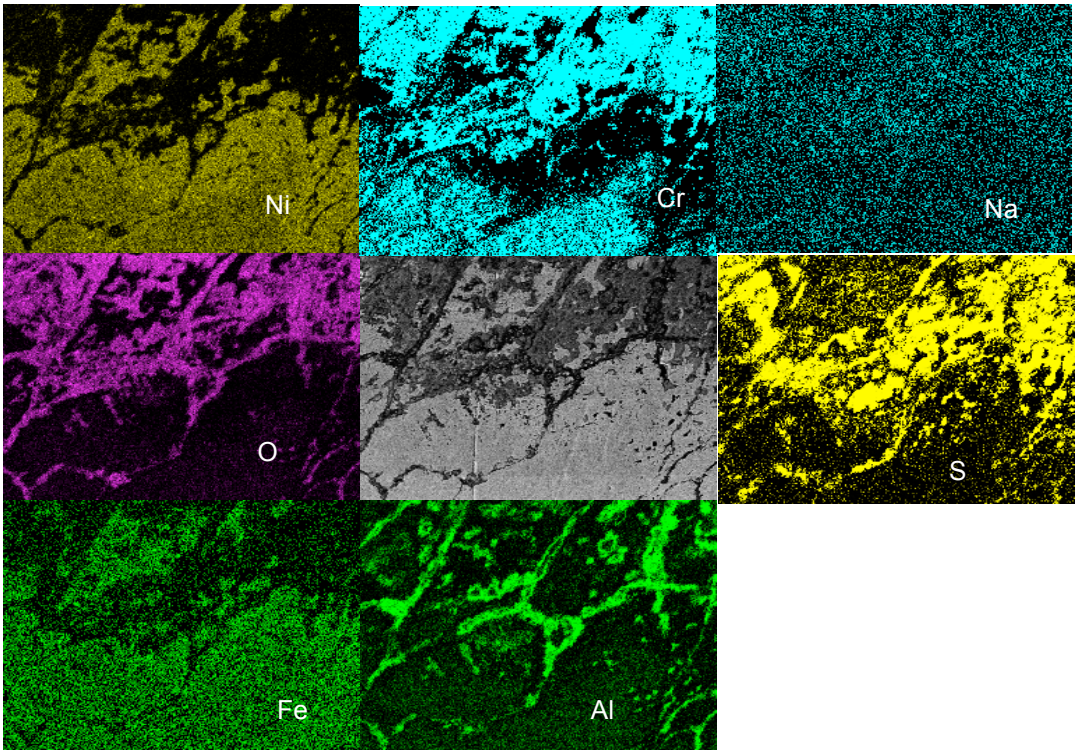

Figure 10. EDX mapping of the corroded cross section of Alloy 693, after 6300-h exposure to Gas A and ash at 750°C.

In the non-corroded region (see Fig. 11), the EDX analysis shows a somewhat protective Cr oxide on the alloy surface. The ash at the exterior of Cr oxide shows Na, Al, and O, indicating breakdown of sodium sulfate and may be formation of Na aluminate. The sulfur that is released from the sulfate breakdown seems to penetrate along grain boundaries into the alloy substrate. This is a classical scale morphology in which the oxide scale is fairly protective towards corrosion and with minor internal sulfidation. The alloy also shows a continuous inner layer of Al oxide as expected based on the alloy chemical composition.

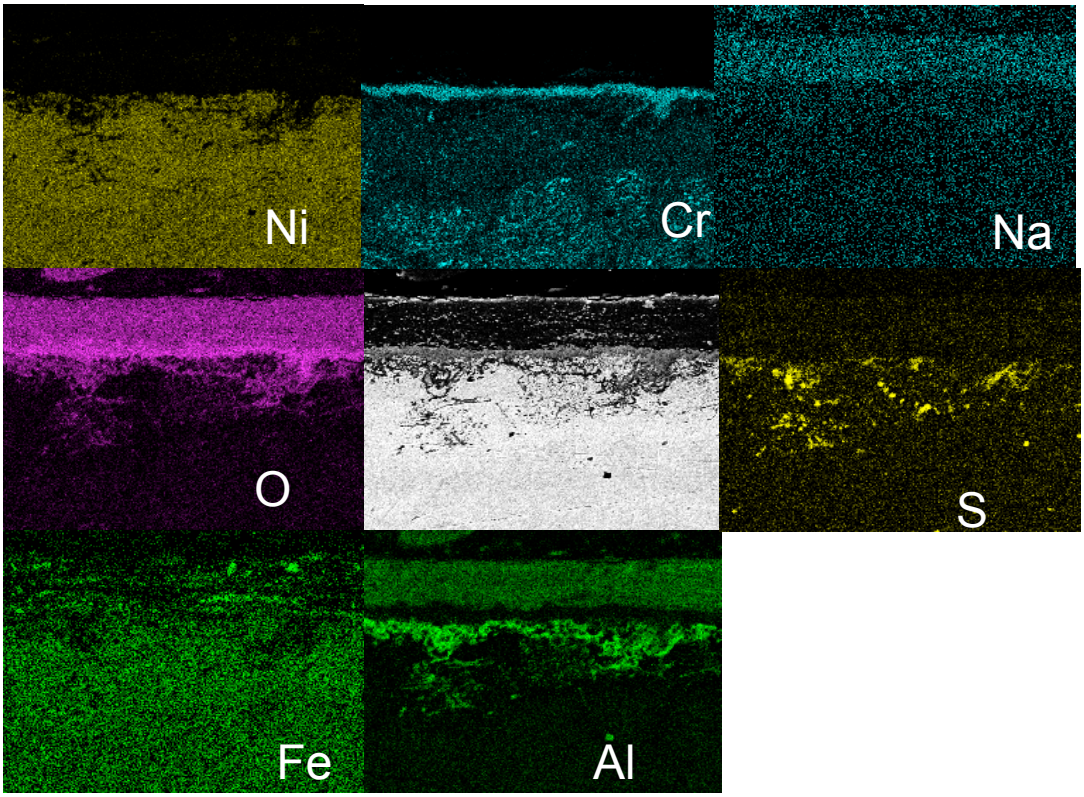

Figure 11. EDX mapping of the non-corroded cross section of Alloy 693, after 6300-h exposure to Gas A and ash at 750°C.

Effect of Ash Chemistry on Corrosion

The ash chemistry and its characteristics in U.S. coals strongly depend on whether the coal is mined in the eastern and midwestern (Illinois, Kentucky, West Virginia, Ohio, etc.) parts of the country or in the western (Montana, Wyoming, etc.) parts of the country. The eastern coals, in general, are high in sulfur and the ash contains predominantly alumina, silica, and iron oxide. The western coals are generally low in sulfur and high in alkalis and the ash contains alumina, silica, and calcium oxide with small amount of iron oxide.

In the ongoing corrosion program in support of oxy-fuel combustion systems, we have examined the role of ash chemistry that simulates both eastern and western coals. Over the past few years, the tests were conducted with ash that simulated eastern coals. During the current year, we have initiated corrosion tests in the presence of ash that simulated western coals.

As discussed earlier in this paper, the synthetic coal-ash deposit, that simulates ash from eastern coal, consisted of a mixture of reagent-grade SiO_2, Al_2O_3, and Fe_2O_3 in the ratio of 1:1:1 by weight. The alkali sulfate mixture consisted of Na_2SO_4 and K_2SO_4 in the ratio of 1:1 by weight. The corrosion test results conducted with eastern coal ash were reported in earlier conference papers [4, 5] and in Section 3 of this paper.

The synthetic coal-ash deposit, that simulates ash from western coal, consisted of a mixture of reagent-grade 36%SiO_2-16%Al_2O_3, 9%Fe_2O_3, and 29%CaO. The alkali sulfate mixture consisted of Na_2SO_4 and K_2SO_4 in the ratio of 1:1 by weight in the ratio of 1:1:1 by weight. One of the key considerations with the western coal ash is that calcium (if present in the desirable form) may getter the sulfur and may result in a relatively lower sulfur environment, thereby, minimize the corrosion of metallic materials.

Figure 12 shows the stability of CaO, CaS, and $CaSO_4$ phases as a function of oxygen and sulfur partial pressures at 704, 840, and 900°C. The dashed curve at 900°C is the gas equilibria projected for fluidized bed combustion environment, typical of coal-fired bubbling beds [7]. The phase stability data in Figure 12 shows that in the anticipated pO_2 and pS_2 in oxy-fuel combustion systems, the most stable phase would be $CaSO_4$. One of the concerns with Ca in the coal ash is the potential change in its chemical stability as the ash particles cool from the combustion temperature of 1300-1500°C to the deposit temperature (600-800°C) on superheater tube walls.

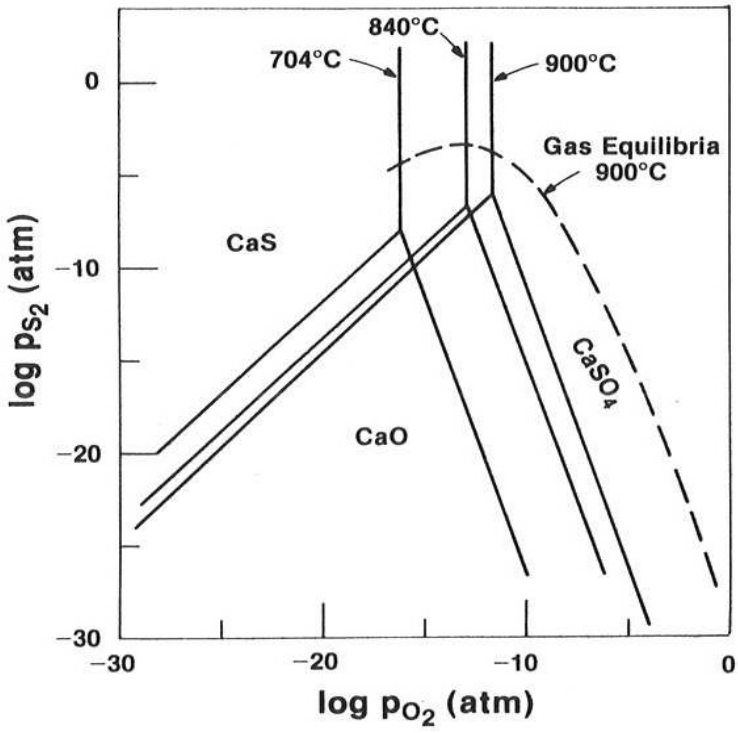

Figure 12. CaO-CaS-$CaSO_4$ phase stability fields calculated for several temperatures. Dashed curve represents thermodynamic gas-phase euilibria in combustion atmosphere.

To examine the chemical form of Ca in the ash (especially after combustion at elevated temperatures >1100°C), we have sintered the ash mixture at 1100°C in air and analyzed the sintered ash using X-ray diffraction. Figure 13 shows the XRD data, indicating the Ca-

containing phases as $CaSiO_3$, $CaAl_2O_4$, $Ca_2Al_2SiO_7$, and $Ca_3Si_2O_7$. The predominant phases are $CaAl_2O_4$ and $Ca_2Al_2SiO_7$. Based on these results, it can be concluded that the Ca in coal ash would react with Si and Al to form these ternary and quaternary compounds and the sulfur capture capacity of these Ca-containing compounds would dictate the extent of SO_2 in the gas environment at the superheater section of the plant. Figure 14 shows the XRD of the initially-sintered synthetic coal ash after exposure in corrosion experiment at 750°C in the presence of Gas A (with steam) and Gas B (without steam). The phases in the ash after 300-h exposure in corrosion experiment are $CaSO_4$, SiO_2, and Fe_2O_3 with a preponderance of $CaSO_4$. The results show that the compounds containing Ca, Si, and Al (shown in Fig. 13) have reacted with SO_2 in the corrosion experiment to form $CaSO_4$, which is encouraging for sulfur capture and possible reduction of corrosion of superheater materials.

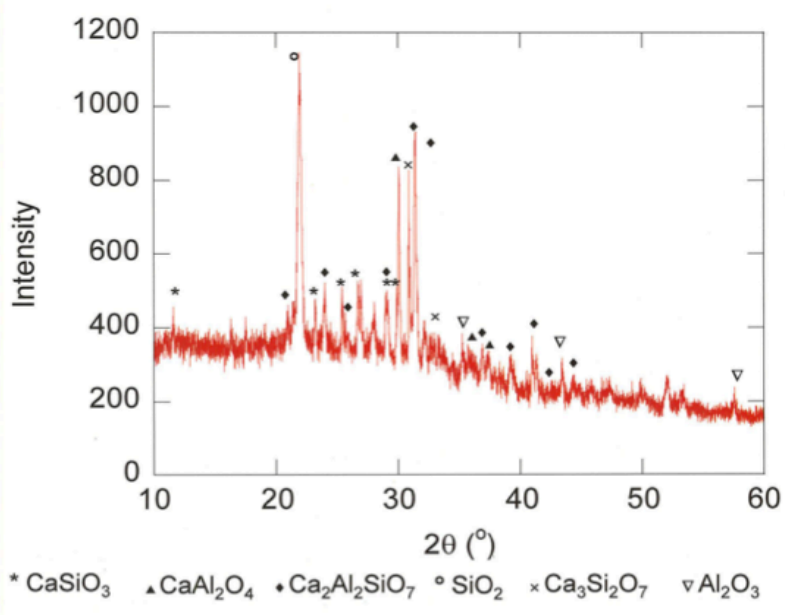

Figure 13. XRD of synthetic ash (simulating US Western coal) after sintering at 1100°C.

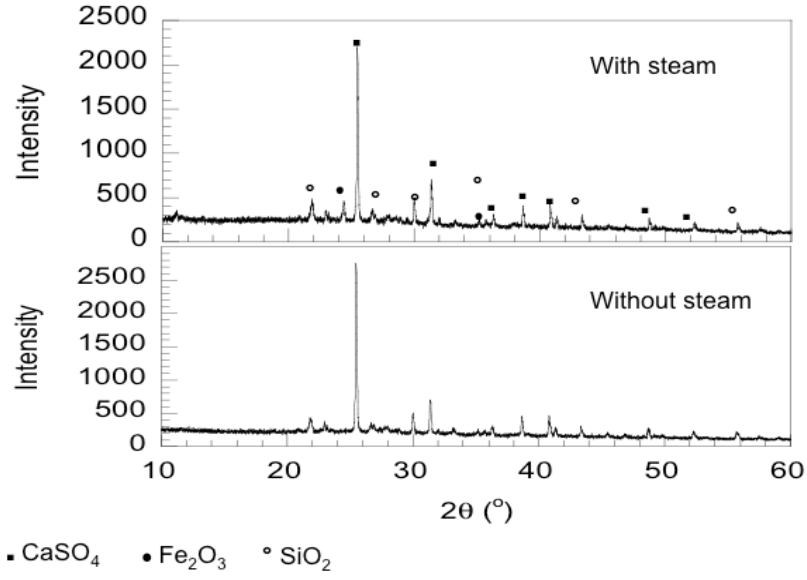

Figure 14. XRD of initially sintered synthetic ash (simulating US western coal) after exposure to (top) Gas A and (bottom) Gas B in corrosion experiments.

To examine the stability of stability of Ca containing phases and their reaction with SO_2 to form $CaSO_4$, thermodynamic calculations were made at several temperatures to establish pSO_2-temperature diagram for various reactions. Figure 15 shows the stability regions for various reactions. Also shown in the figure is the stability region for $CaCO_3$ (limestone) reaction with SO_2 to form $CaSO_4$. The dashed line in the figure corresponds to the SO_2 level in the corrosion experiment, which is anticipated in the oxy-fuel combustion systems. The results indicate that all the Ca-containing compounds will react with SO2 in the combustion environment to getter sulfur in the gas up to ≈1000°C.

At present long-term corrosion experiments are being conducted in the presence of ash simulating western coal and the results will be compared with the data generated with eastern coal ash. It is also planned to procure ash from oxy-fuel combustion pilot plants and commercial systems and use them in performing corrosion tests.

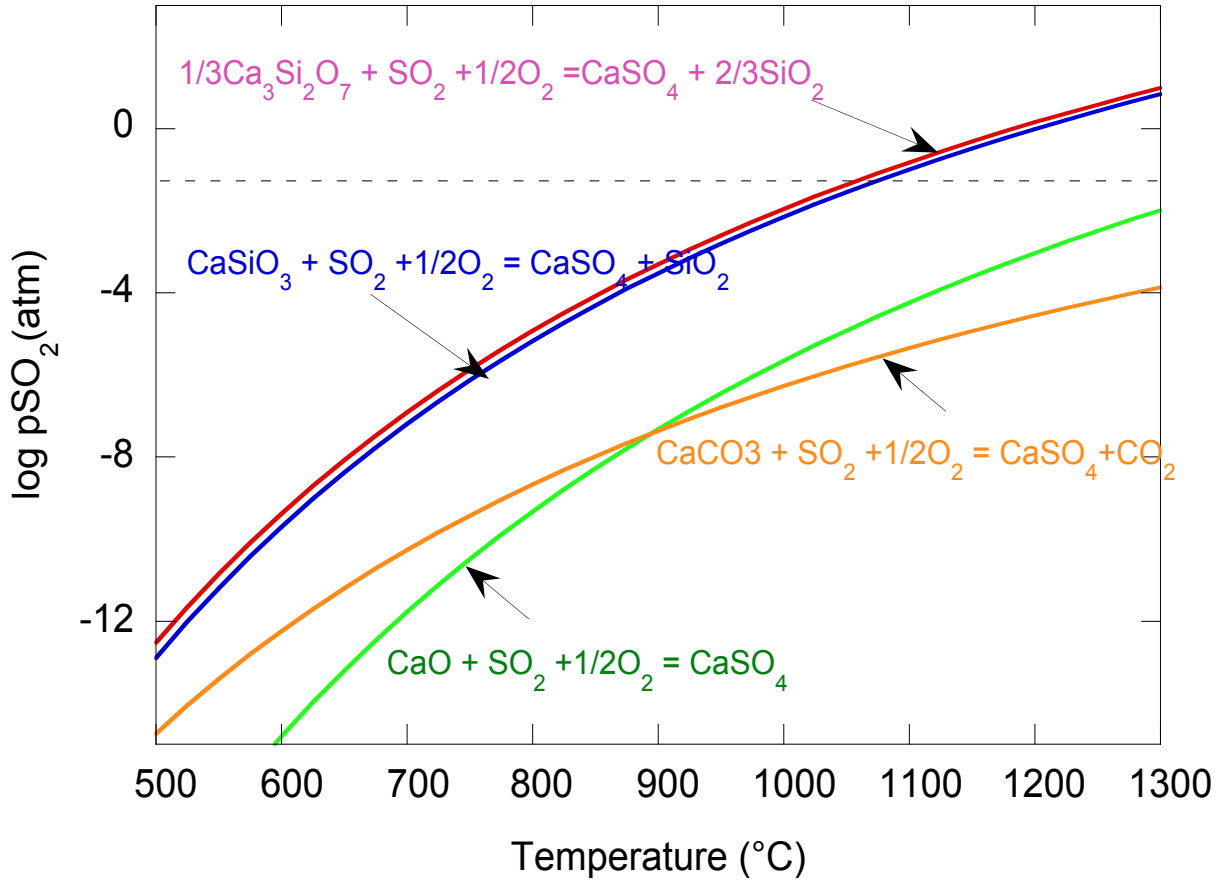

Figure 15. Thermodynamic stability of various phases that can occur due to chemical reactions at various temperatures. The dashed line indicates the pSO_2 used in the corrosion experiments.

Summary

We have conducted a detailed study at Argonne National Laboratory, to evaluate the oxidation performance of structural alloys at 750°C in simulated oxy-fuel environments in the presence of

synthetic ash and sulfur-containing gaseous environments. Corrosion rates in the environments with ash are much higher than those obtained in the absence of ash. The presence of ash (with alkali sulfates) coupled with steam in the gas environment accelerates corrosion of all structural alloys. The observed corrosion rates in ash environments are higher than what is acceptable for many alloys. Among the alloying elements, Nb, Mo, W, and Al in alloys accelerate the corrosion rate in ash environment. Localized corrosion was observed in both environments with ash and without ash. Alloys exhibit an incubation period for ash corrosion during which the corrosion rate is low. Upon exceeding the incubation period, metallic network structure develops and corrosion accelerated. This is based on the microstructural examination of the tested specimens for internal oxidation/sulfidation/penetration of the substrate alloys. The effect of steam on the incubation time depends on alloy composition.

In typical oxy-fuel combustion environments used in this study, most of the alloys exhibit corrosion rates ≥2 mm/year, based on linear kinetics. Long-term experiments have been conducted in the presence of synthetic coal ash simulating eastern coal and results have been reported. Preliminary test results are presented on the corrosion performance of alloys after exposure to Ca-containing ash that simulates western coal.

Acknowledgements

This paper was presented at the 26th Annual Conference on Fossil Energy Materials, Pittsburgh, PA, April 17-19, 2012. This work was supported by the U.S. Department of Energy, Office of Fossil Energy, Advanced Research Materials Program, Work Breakdown Structure Element ANL-4, under Contract DE-AC02-06CH11357.

References

1. K. Natesan and D. L. Rink, "Corrosion Performance of Structural Alloys for Oxy-fuel Combustion Systems," Proc. 21st Annual Conference on Fossil Energy Materials, Knoxville, TN, April 30- May 2, 2007.

2. K. Natesan, Z. Zeng, and D. L. Rink, "Materials Performance of Structural Alloys in CO_2 and in CO_2-Steam Environments," Proc. 22nd Annual Conference on Fossil Energy Materials, Pittsburgh, PA, June 8-10, 2008.

3. K. Natesan, Z. Zeng, and D. L. Rink, "Materials Performance of Structural Alloys in CO_2 and in CO_2-Steam Environments," paper presented at the 23rd Annual Conference on Fossil Energy Materials, Pittsburgh, PA, May 12-14, 2009 and published in the conference proceedings.

4. K. Natesan, Z. Zeng, and D. L. Rink, "Materials Performance of Structural Alloys in Simulated Oxy-fuel Environments," paper presented at the 24rd Annual Conference on Fossil Energy Materials, Pittsburgh, PA, May 25-27, 2010 and published in the conference proceedings.

5. K. Natesan, Z. Zeng, and D. L. Rink, "Effect of Gas Composition on Materials Performance of Structural Alloys in Simulated Oxy-fuel Environments," paper presented at the 25th Annual Conference on Fossil Energy Materials, Portland, OR, April 26-28, 2011 and published in the conference proceedings.

6. B. A. Baker and G. D. Smith, Paper 04526, presented at the NACE Annual Conference 2004, New Orleans, LA, March 28-April 1, 2004.

7. K. Natesan, "Role of FBC Deposits in the Corrosion of Heat Exchanger Materials," High Temperature Technology, Vol. 4(4), 193, 1986.